JOURNAL OF Applied Polymer SCIENCE

Enhanced Foamability of Isotactic Polypropylene Composites by Polypropylene-Graft-Carbon Nanotube

Chen Chen,[1] Huan Pang,[2] Zhong Liu,[3] Yu-Bao Li,[1] Yan-Hui Chen,[2] Wei-Qin Zhang,[2] Xu Ji,[4] Jian-Hua Tang[4]

[1]Research Center for Nano-Biomaterials, Analytical and Testing Center, Sichuan University, Chengdu, Sichuan, 610065, China
[2]State Key Laboratory of Polymer Materials Engineering, College of Polymer Science and Engineering, Sichuan University, Chengdu, Sichuan 610065, China
[3]The First People's Hospital of Longquanyi District, Chengdu, Sichuan, 610100, China
[4]College of Chemical Engineering, Sichuan University, Chengdu, Sichuan, 610065, China
Correspondence to: C. Chen (E-mail: cdcc@scu.edu.cn)

ABSTRACT: In this article, utilizing a nucleophilic substitution reaction between epoxy group in polypropylene-graft-glycidyl methacrylate (PP-*g*-GMA) and carboxyl groups in oxidized carbon nanotubes (O-CNTs), PP-*g*-CNT was fabricated for reinforcing the interfacial adhesion between CNTs and polypropylene (PP) matrix, favoring the enhancement of melt strength and elastic modulus, i.e., enhancing the foaming ability of PP composites. Cellular structure and thermo-mechanical properties of PP foams were characterized by scanning electron microscopy and dynamic mechanical analysis, respectively. The average cell diameter of PP foams decreased from 289.2 (PP-*g*-GMA) to 96.7 μm (PP-*g*-CNT foams with 2.0 wt % O-CNT) and the distribution of cell size also became more uniform. The storage modulus of PP-*g*-CNT foams increased by nearly 62.5% at -40°C, compared with that of PP-*g*-GMA foams. This work also provided a new procedure for improving the foam ability and thermo-mechanical property of PP composites. © 2013 Wiley Periodicals, Inc. J. Appl. Polym. Sci. 130: 961–968, 2013

KEYWORDS: mechanical properties; foams; crystallization

Received 25 December 2012; accepted 24 February 2013; published online 17 April 2013
DOI: 10.1002/app.39232

INTRODUCTION

Thermoplastic foam materials, such as polystyrene and polyethylene, are widely used in a variety of applications for the advantages of their energy absorption characteristics, thermal properties, and specific strength.[1] However, there are some disadvantages in the performance of traditional thermoplastic foams, for example, the low softening temperature (below $\sim 80^{\circ}$C) of PS and inferior mechanical property of PE. Thus, the practical applications of these thermoplastic foams are restricted.[2,3] Isotactic polypropylene (iPP) foam attracts enormous attentions from many researchers, because of its high melting temperature, chemical resistance, stiffness, and high compressive strength.[4] so iPP foams are very likely to replace other thermoplastic foams in various practical applications.[3–6] However, the foaming property of ordinary linear iPP is limited by its low melt strength (MS), which easily causes a cell elongation defect during cell growth.[7–10] In general, the key to improving the foaming property of iPP is to obtain high MS. There are three effective methods to improve MS of iPP widely reported in literature:[1,11–20] (1) addition of nanoparticles in polymer matrix; (2) introduction of long chains branched (LCB) iPP chains; (3) crosslinking of iPP chains, which all can stabilize the bubbles' growth and avoid the cell coalescence or rupture during the foaming process. Nofar et al. studied the foaming ability of linear iPP with nanoclay and coupling agent, and it was found that the introduction of nanocaly and coupling agent largely improved the foam cell density and expansion ratio.[11] Li et al. introduced long chain branches to commercial iPP using an extender agent to couple with glycidyl methacrylate-grafted iPP (PP-*g*-GMA), and observed the foam ability of LCB iPP was significantly enhanced.[14] Tang et al. utilized copper *N,N*-dimethyldithiocarbamate to control the melt reaction during the preparation of LCB iPP via free radical grafting, and the obtained LCB iPP composites displayed high MS, leading to the excellent foam ability.[15] Liu et al. investigated the influence of silane crosslink on the foaming properties of iPP foams, and they found that the MS value of PP was increased by $\sim$360% compared with that of neat iPP, corresponding to the improvement

© 2013 Wiley Periodicals, Inc.

of iPP foaming processability.[1] Nojiri et al. modified iPP by mixing iPP with crosslinking agent in an extruder, followed by γ-radiation to induce the iPP chains cross-linking to obtain high MS.[20] Although numerous investigations focused on the fabrication of high MS iPP, to date, it still remains a considerable challenge to achieve their large-scale industrial productions. Fundamental and applied studies on manufacturing high MS iPP and improving its foaming ability are therefore of continuing interesting.

In this work, we introduced a new and facile methodology to enhance the foaming ability of iPP, namely, via a nucleophilic substitution reaction between PP-*g*-GMA and oxidative carbon nanotubes (O-CNTs), iPP chains were grafted to surfaces of O-CNTs. The MS of iPP can be dramatically improved by the presence of PP-*g*-CNT, as a result of the enhanced foaming ability of iPP. The influence of PP-*g*-CNT on the thermo-stability, isothermal crystallization, thermo-mechanical and thermal conductivity was also studied.

EXPERIMENTAL

Materials

The commercial grade linear iPP particles were supplied by Ningxia petrochemical (Yinchuan, China) with a melt flow rate of 40 g/10 min (230°C, 21.6 N) and $\rho = 0.90$ g/cm^3. Raw CNTs (20–40 nm diameter, 10–20 μm length and O/C = 0.012) were supplied by Chengdu Organic Chemicals (Chengdu, China). The compound blowing agent (DDL101) composed of azodicarbonamide in powder with a diameter of ~10 μm was friendly donated by Qingdao Dandelin (Qingdao, China), and its decomposition temperature agent is ~200°C. Commercial grade dicumyl peroxide (DCP) was supplied from Ciba, German. Xylene [analytical reagent (AR) grade], nitric acid (HNO_3) (AR grade), hydrogen peroxide (H_2O_2) (AR grade), and alcohol (AR grade) were purchased from Chengdu Kelong Chemical Reagent Factory (Chengdu, China) and used as received. PP-*g*-GMA was synthesized in our laboratory using the methods reported by Pazzagli and Pracella,[21,22] i.e., melting radical grafting reaction of iPP with GMA monomer and radical initiator of DCP. In order to increase both grafting rate and yield of PP-*g*-GMA and, in the meantime, reduce iPP chain scission, styrene monomers were also added to the iPP/GMA/DCP reacting system. Due to the limitation of *in situ* extrusion reaction process, the obtained PP-*g*-GMA is actually a mixture of PP-*g*-GMA and iPP matrix. The GMA grafting conversion is ~16% measured by titration method. O-CNTs were prepared by oxidizing the pristine CNTs with HNO_3 and H_2O_2. The raw CNTs were firstly treated by 3.0 mol/L HNO_3 for 2 h and then 30% (v/v) H_2O_2 for another 2 h.[23]

Preparation of PP Foam Composites

As illustrated in Figure 1, to achieve the desirable dispersion, PP-*g*-GMA and O-CNTs were firstly blended via a simple melt compounding method using an internal mixer. In order to guarantee a complete conversion of the nucleophilic substitution reaction, the mass ratio of O-CNT/PP-*g*-GMA was determined at 1/200 and 1/50, respectively.[24] The final product prepared was the mixture of PP-*g*-CNT and PP-*g*-GMA. Then, the mixture was solved in xylene, followed by ethanol flocculation. The PP-*g*-CNT/PP-*g*-GMA compound was filtered and dried in a vacuum oven for 48 h at 60°C. The dried mixture was mechanically pulverized to grains with a diameter of ~20 μm. The PP-*g*-CNT grains, 4 wt % blowing agent DDL-101 and 0.2 wt % antioxidants were mixed in a high speed mixer for 4 min at a speed of 25,000 rmp. The mixture was compressed at 200°C and 10 MPa for 8 min. After unloading the pressure and cooling to room temperature, the PP-*g*-CNT foams were obtained. For the control samples of PP-*g*-GMA foams, the

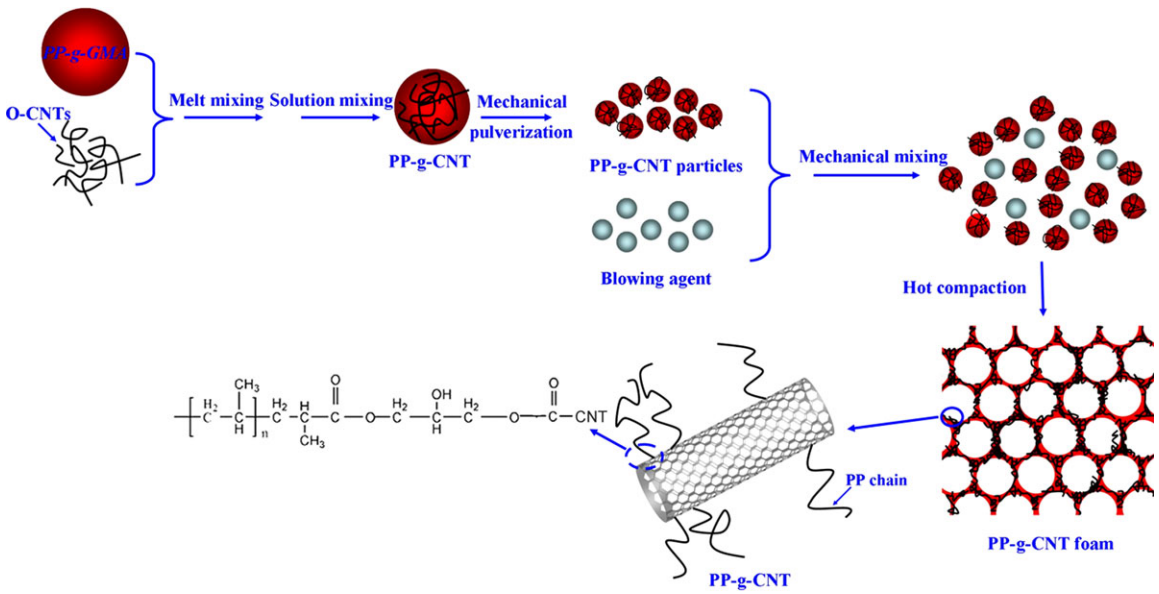

Figure 1. Schematic for the fabrication of the PP-*g*-CNT foam. [Color figure can be viewed in the online issue, which is available at wileyonlinelibrary.com.]

process was the same as that of PP-*g*-CNT samples. The PP-*g*-CNT composites with 0.5 and 2.0 wt % O-CNT loadings were noted as PPCN05 and PPCN20, respectively.

Characterization

The cellular morphology of samples was observed under a Field-emission scanning electron microscopy (SEM) (Inspect F, FEI, Finland) with an accelerating voltage of 20 kV. The SEM samples were prepared by immersing the bulks in liquid nitrogen for 30 min before fracture. Fourier transform infrared (FTIR) spectra were obtained using a Nicolet-560 FTIR spectrometer (Nicolet Corp., USA). For the FTIR characterization, The PP-*g*-CNT mixture was extracted with boiling xylene for 24 h to remove unreacted PP-*g*-GMA. Thermal conductivity was measured by the transient plane source technique using a Hot Disk 2500-OT equipment (Hot disk AB, Sweden) at room temperature according to ASTM C518-91. Differential scanning calorimetry (DSC) measurement of PP-*g*-CNT composites was carried out on a TA Instruments' Q200 under a nitrogen flow, which was calibrated by indium as the standard. For the isothermal crystallization, the samples were annealed at 180°C for 5 min to eliminate thermal history, then cooled to crystallization temperature (T_c) at a rate of 20°C/min, and maintained at T_c until the crystallization was completed. Thermogravimeric analysis (TGA) measurement was conducted under N_2 flow using Netzsch-TG209F1 instrument at a heating rate of 5°C/min and a nitrogen flow of 50 cm^3/min. Dynamical Mechanical Analysis (DMA) analyses were carried out with a Q800 DMA instrument (TA Instruments, USA) at a heating rate of 5 °C/min. The testing temperature range was from −40 to 140 °C. The viscoelastic properties of the PP-*g*-GMA and PP-*g*-CNT samples were studied with a stress controlled dynamic rheometer AR2000ex (TA, USA), using a parallel plate geometry. The dynamic rheological tests of the samples with a thickness of ~1 mm were then conducted at 200°C. The gap used for rheological measurements was ~800 μm. The strain and oscillation frequency range used were 1.0% and 0.01–100 Hz, respectively.

The density of foams was measured by the water displacement method, and the cell density and mean diameter was calculated from the SEM micrographs at a magnification of ×100. Three zones, each of which contained about 50 cells were selected randomly from the SEM micrographs of each sample and analyzed using Nano Measurer 1.2 Program. The cell density (N_0) was calculated with the following equation:

$$N_0 = \left[\frac{n}{A}\right]^{3/2} \quad (1)$$

where n is the number of cell projections in the defined image area A, derived from SEM micrographs.

RESULTS AND DISCUSSION

Figure 2(a) shows the morphology of the curved and coiled O-CNTs used in this work, which confirms the preservation of the large aspect ratio of O-CNTs after oxidized modification compared to raw CNTs [Figure 2(b)].[25] The FTIR spectrum of raw CNTs and O-CNTs are displayed in Figure 3. The new peaks at 1718 cm^{-1} of O-CNTs compared with raw CNTs is responsible for the C=O stretching vibration, indicative of the successful introduction of carbonyl groups to the surfaces of O-CNTs.[26] The broad peak at 3440 cm^{-1} corresponds to the stretching vibration of hydroxyl group. While for PP-*g*-GMA, the peaks at 1375 cm^{-1} and 1455 cm^{-1} are both assigned to bending vibration of CH_3, the advent of peak at 1718 cm^{-1} is attributed to C=O stretching vibration because of oxidation process, and the peak around 2920 cm^{-1} represents the stretching vibration of C—H.[27] For the FTIR curve of CNT-*g*-PP, the peaks at 1375 cm^{-1}, 1455 cm^{-1}, and 2920 cm^{-1} all appear, demonstrating that PP-*g*-GMA has been grafted onto O-CNTs during the melt process.[27] In addition, the blue shift of C=O stretching vibration from 1718 to 1688 cm^{-1} can also confirm the covalent bonding of PP chains onto the CNT surfaces, which is consistent with the previous work by Li et al.[28]

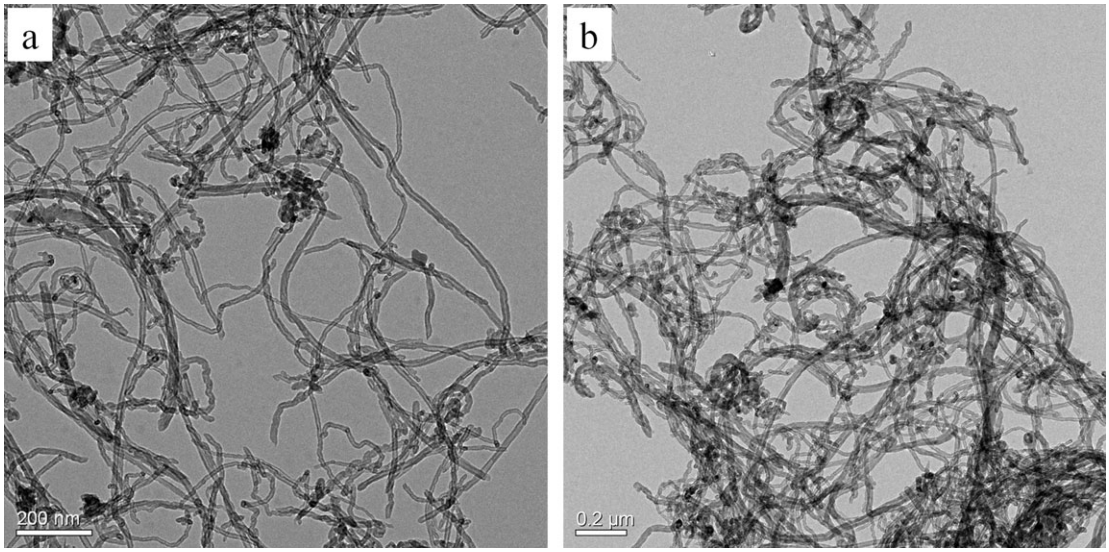

Figure 2. TEM images of as-prepared O-CNTs (a) and raw CNTs (b).

Applied Polymer SCIENCE

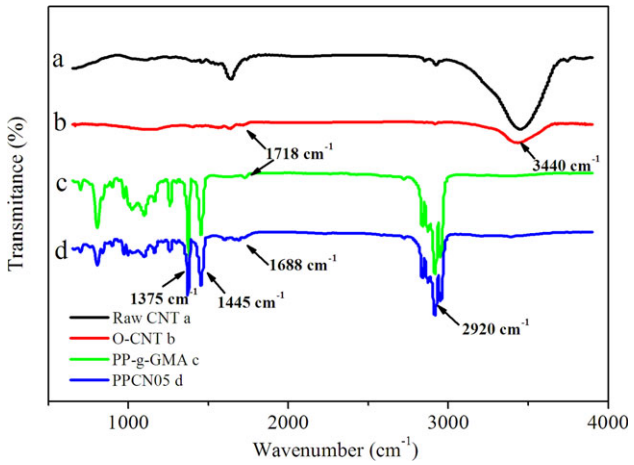

Figure 3. FTIR spectra of (a) raw CNTs, (b) O-CNTs, (c) PP-*g*-GMA and (d) PPCN05 sample. [Color figure can be viewed in the online issue, which is available at wileyonlinelibrary.com.]

Figure 4(a) shows DSC curves of PP-*g*-GMA and PP-*g*-CNT composites during isothermal crystallization at 138°C. After a short-lived induction period, the exothermic curves shifted along the time axis, gradually reached the maximum peak and then returned to the platform. The half crystallization time ($t_{1/2}$) was respectively reduced to 41.2% and 49.8% of PPCN05 and PPCN20 samples, compared to that of PP-*g*-GMA. Apparently, the accomplishment of the crystallization process for PP-*g*-CNT composites was faster than that of PP-*g*-GMA. As shown in Figure 4(b), $t_{1/2}$ of PP-*g*-GMA raised rapidly with increasing T_c, corresponding to the decrease of crystallization rate. Such variation implies that the isothermal crystallization kinetics of PP-*g*-GMA is a nucleation control process. In contrast, $t_{1/2}$ of PPCN05 and PPCN20 displays a slight increase in the isothermal temperature range of 132–142°C, indicative of lower temperature sensitivity of crystallization rate. In addition, there was little difference between PPCN05 and PPCN20 for all other kinetic measurements, especially at low supercooling degree. This result indicates that 0.5 wt % PP-*g*-CNT can offer sufficient surface area for crystallite nucleation, which is in line with other literature.[29,30]

Figure 5 shows the elastic modulus of PP-*g*-GMA and PP-*g*-CNT samples, which can manifest the magnitude of MS. Apparently, PP-*g*-CNT led to a considerable increase in elastic modulus than that for PP-*g*-GMA. With the increase of frequency, PP-*g*-GMA had a drastic sensitivity of elastic modulus to frequency, while PPCN05 and PPCN20 depressed the frequency dependence of the elastic modulus. Especially, the PPCN20 sample was nearly independent of frequency. The lower frequency sensitivity indicates that PP-*g*-CNT tended to construct a network structure.[31] This significant increase of elastic modulus is ascribed to the two following reasons: the presence of PP-*g*-CNT with a large aspect ratio constrained the mobility of PP chains, since only a small amount of PP-*g*-CNT (~2.0 wt %) formed a nanotube network in polymer matrix and made the composite rheological behavior change from liquid-like to solid-like according to Pötschke, et al.[31] Another reason was the

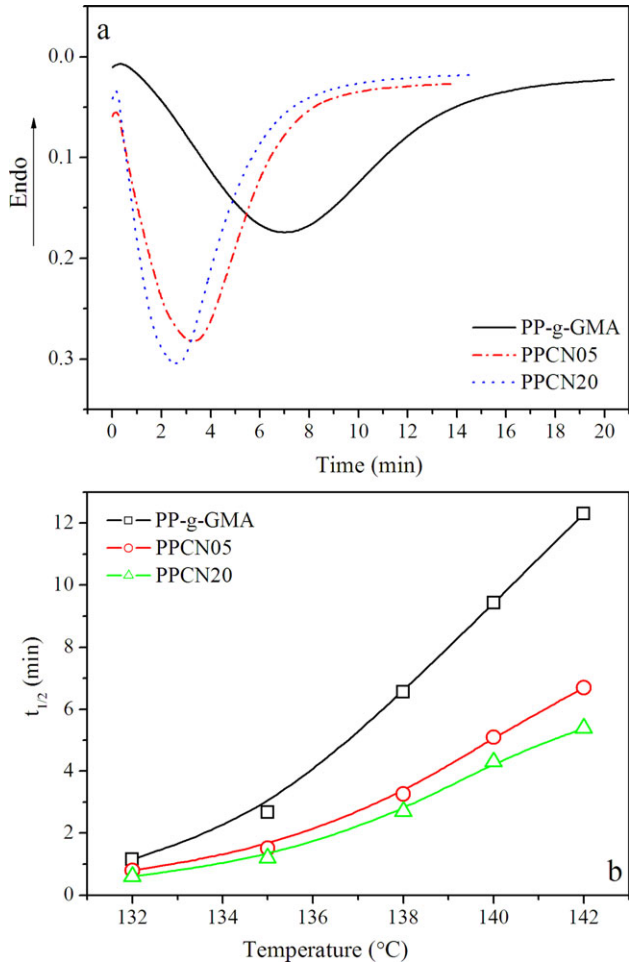

Figure 4. DSC curves of PP-*g*-GMA, PPCN05, and PPCN20 during isothermally crystallizing at 138°C (a); plots of $t_{1/2}$ against different T_c (b). [Color figure can be viewed in the online issue, which is available at wileyonlinelibrary.com.]

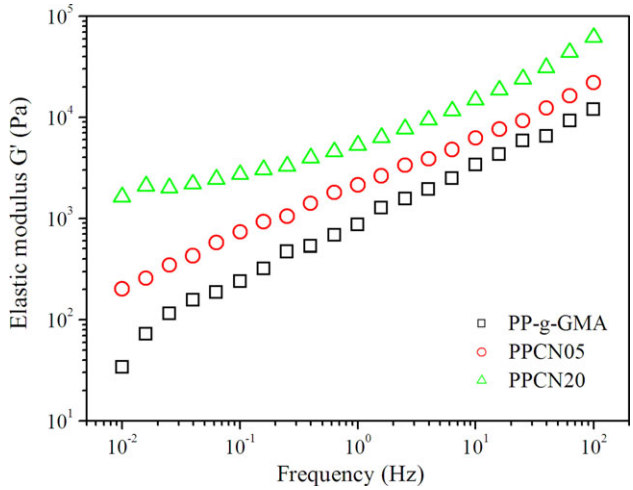

Figure 5. Viscoelastic properties of PP-*g*-GMA, PPCN05, and PPCN20 samples. [Color figure can be viewed in the online issue, which is available at wileyonlinelibrary.com.]

intensive interface interaction between PP-*g*-CNT and iPP, because of the excellent compatibility between the grafted iPP chains of PP-*g*-CNT and iPP matrix, which also resulted in a more uniform dispersion of nanotubes.

Figure 6 shows the SEM micrographs of PP-*g*-GMA and PP-*g*-CNT foam composites, respectively. The SEM images of PP-*g*-GMA foam samples [Figure 6(a)] display the evidence of severe cell coalescence and large scale in-homogeneity of cells, indicative of low melt strength of polymer melt during foaming. When the loading of nanotubes was 0.5 wt %, the quality of cell structure was largely improved; however, most of the cells were larger than 120 μm. When the concentration of PP-*g*-CNT increased to 2.0 wt %, PPCN20 foam possessed better cellular structure than that for PPCN05. Moreover, the effect of PP-*g*-CNT on foam quality can be understood by comparing the cell size distribution shown in Figure 7. Compared with the broad cell size distribution of PP-*g*-GMA (30–200 μm), the cell size distribution presented for PPCN05 and PPCN20 was distinctly narrower with most cells in the range of 40–160 and 20–130 μm. As listed in Table I, the decreased density (0.16 to 0.10 g/cm^3) and increased cell density (from 0.9×10^5 to 4.5×10^5) also reveal the enhanced foaming ability. The improvement in foam quality of PP-*g*-CNT foams can be attributed to the increased melt strength and larger surface area for heterogeneous nucleation in PP-*g*-CNT samples than that of PP-*g*-GMA.[32]

The thermal stability of O-CNTs and PP-*g*-CNT foam composites was investigated by TGA in nitrogen atmosphere at a heating rate of 5°C/min as shown in Figure 8. More than 12% weight loss for O-CNTs at 800°C indicates the pyrolysis of the oxidative debris that is strongly attached onto nanotube surfaces. For further evaluating the initial thermal stability of PP-*g*-CNT samples, temperatures at which 5% weight loss occurs, referred as $T_{-5\%}$, is employed. The presence of PP-*g*-CNT has a positive effect on the thermal stability of the composites. $T_{-5\%}$ of PPCN20 was 25.2°C higher than that of PP-*g*-GMA (364°C), and 7.9°C higher than that of PPCN05 (the inset of Figure 8). This prominent improvement even at the low PP-*g*-CNT loading is attributed to the decreased interfacial thermal resistance between PP-*g*-CNT and iPP matrix, resulting from the high aspect ratio, superior thermal

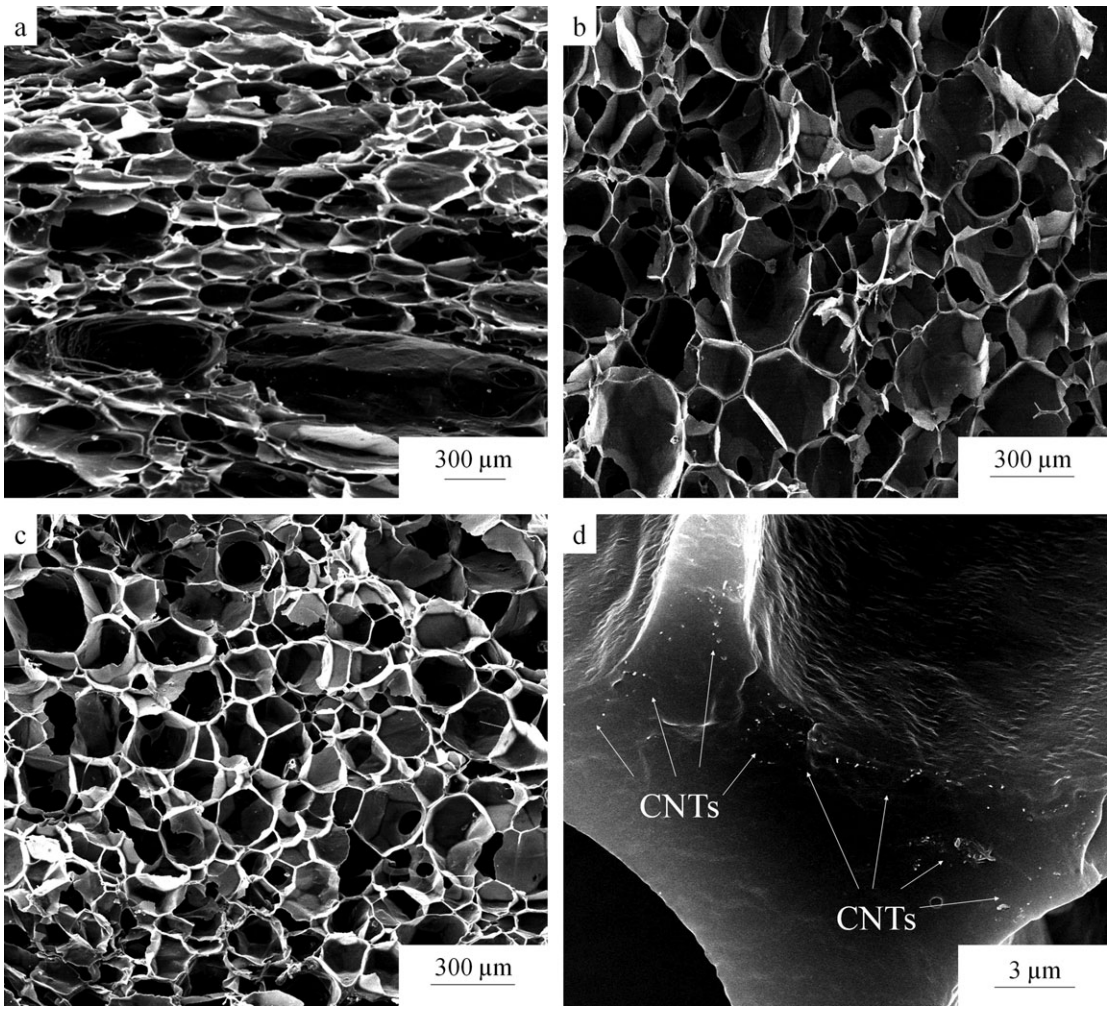

Figure 6. SEM micrographs of the cryofractured PP-*g*-GMA (a), PPCN05 (b), PPCN20 (c), and the high-magnification image (d) of a cell wall in PPCN20.

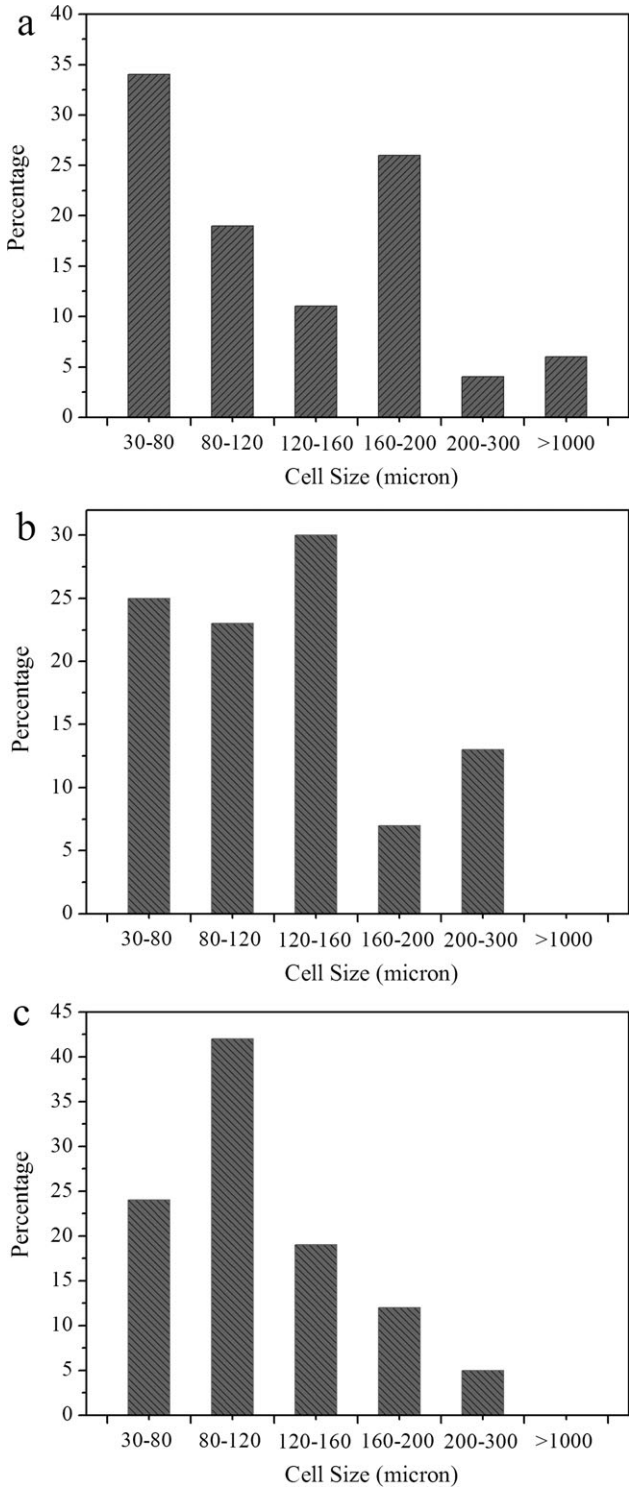

Figure 7. Cell size distributions in PP-*g*-GMA (a) PPCN05 (b) and PPCN20 (c).

conductivity of PP-*g*-CNT and the excellent interfacial adhesion between PP-*g*-CNT and iPP matrix.[28]

Figure 9 shows DMA temperature scans at 5 Hz frequency for PP-*g*-GMA and PP-*g*-CNT foams. Storage modulus (E') for all

Table I. Density, Cell Size, and Cell Density of PP-*g*-GMA and PP-*g*-CNT Foams

Sample	Density (g/cm^3)	Cell size (μm)	Cell density ($no./cm^3$)
PP-*g*-GMA	0.16	280	0.9×10^5
PPCN05	0.11	130	2.6×10^5
PPCN20	0.10	97	4.5×10^5

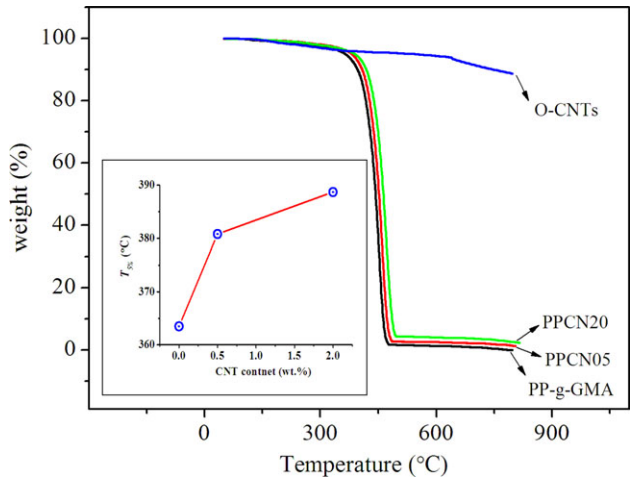

Figure 8. TGA analyses of O-CNTs, PP-*g*-GMA, and PP-*g*-CNT foams. [Color figure can be viewed in the online issue, which is available at wileyonlinelibrary.com.]

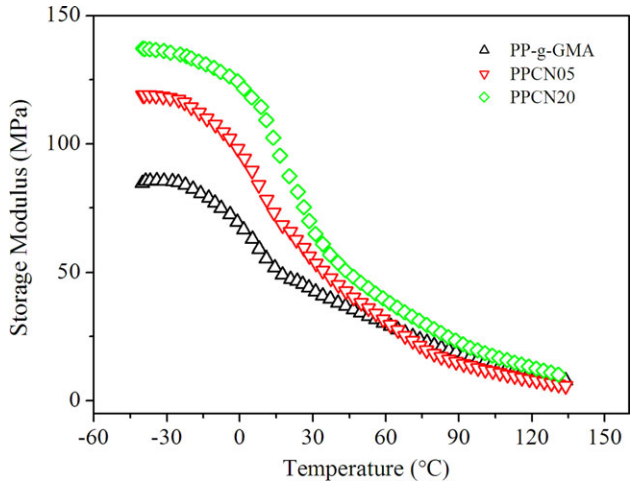

Figure 9. The storage modulus–temperature curves of PP-*g*-GMA and PP-*g*-CNT/PP foams from −40 to 135°C. [Color figure can be viewed in the online issue, which is available at wileyonlinelibrary.com.]

Table II. Thermal Conductivity of PP-*g*-GMA and PP-*g*-CNT/PP Foams

Sample	Thermal conductivity ($\times 10^{-3}$ Wm^{-1} K^{-1})
PP-*g*-GMA	59.8 ± 2.5
PPCN05	48.9 ± 2.8
PPCN20	52.5 ± 1.6

the samples decreased slowly and progressively with temperature in the initial stage from −40 to −20°C and then showed a very rapid decay around 0°C, which correlated with the transition from the glassy to the rubbery state.[31] Interestingly, a large increase in E' could be observed in the PP-*g*-CNT/PP samples compared with the PP-*g*-GMA sample. E' of PP-*g*-CNT/PP foams at −40°C increased nearly 40.5% and 62.0% for PPCN05 and PPCN20, respectively. The marked improvement in storage modulus also indicates a more uniform cellular structure and effective reinforcement of PP-*g*-CNT for PP-*g*-CNT/PP foams than those of the control sample.

For application of the foam composites as a thermal insulator material, the thermal conductivity is a crucial factor. Two competitive aspects could affect the thermal conductivity of PP foam in our case. On one hand, the density influences the total thermal conductivity of foam composites. It has been well established that thermal conductivity generally increases with the density of foams.[33] On the other hand, owing to the superior thermal conductivity of PP-*g*-CNTs, the thermal conductivity of PP foams also increases with the loadings of PP-*g*-CNT. The thermal conductivity of PP-*g*-GMA and PP-*g*-CNT/PP foams is shown in Table II. PP-*g*-GMA foams possessed the thermal conductivity of $\sim 59.8\times10^{-3}$ $Wm^{-1}K^{-1}$, which was higher than that of PPCN05 and PPCN20 (48.9×10^{-3} and 52.5×10^{-3} $Wm^{-1}K^{-1}$ respectively), due to the relatively high density of PP-*g*-GMA. For PP-*g*-CNT foams, the thermal conductivity of PPCN20 foams was slightly higher than that of PPCN05, because of the high PP-*g*-CNT loading. However, the increase of thermal conductivity was limited compared to that of the control sample, which indicates that such loading of PP-*g*-CNT could not hinder the application of PP foams as thermal insulator materials.

CONCLUSIONS

In summary, the chains of PP-*g*-GMA have been successfully grafted onto the surfaces of O-CNTs forming PP-*g*-CNT, through the nucleophilic substitution reactions of residual epoxy and carboxyl groups between GMA and O-CNTs. The foaming ability of PP composites was enhanced in the presence of PP-*g*-CNT, which largely increased the elastic modulus. The average cell diameter of PP foams decreased from 289.2 (PP-*g*-GMA) to 96.7 μm (PPCN20) and the distribution of cell size also became more uniform. Compared with PP-*g*-GMA foams, PP-*g*-CNT/PP foams exhibit a significant enhancement of thermo-mechanical property by an increase of 62.5% at −40°C in storage modulus, due to the more uniform cellular structure and effective reinforcement of PP-*g*-CNT. Furthermore, the PP-*g*-CNT/PP foams can also be applied as thermal insulator foam materials.

ACKNOWLEDGMENTS

The project was funded by the National Natural Science Foundation of China (Contract No. U1162131, 51103089, 51273131 and 21176158). The authors also appreciated the financial support from China Postdoctoral Science special Foundation (2012T50717).

REFERENCES

1. Liu, H.; Chuai, C. Z.; Iqbal, M.; Wang, H. S.; Kalsoom, B. B.; Khattak, M.; Khattak, M. Q. *J. Appl. Polym. Sci.* **2011**, *122*, 973.
2. Wong, C. M.; Tsai, S. J.; Ying, C. H.; Hung, M. L. *J. Cell. Plast.* **2006**, *42*, 153.
3. Xin, C. L.; He , Y. D.; Li, Q. C.; Huang, Y. Z.; Yan, B. R.; Wang, X. D. *J. Appl. Polym. Sci.* **2011**, *119*, 1275.
4. An, Y. J.; Xing, H. P.; Wang, Y. H.; Tang, T. *J. Appl. Polym. Sci.* **2012**, *125*, 2724.
5. Chaudhary, A. K.; Jayaraman, K. *Polym. Eng. Sci.* **2011**, *51*, 1749.
6. Arencón, D.; Antunes, M.; Martínez, A. B.; Velasco, J. I. *Polym. Test.* **2012**, *31*, 217.
7. Saiz-Arroyo, C.; Saja, J. A.; Velasco, J. I.; Rodríguez-Pérez, M. Á. *J. Mater. Sci.* **2012**, *47*, 5680.
8. Stumpf, M.; Spörrer A.; Schmidt, H. W.; Alstädt, V. *J. Cell. Plast.* **2011**, *47*, 519.
9. Seyed, H. T.; Pierre, J. C.; Abdellah, A. *Polym. Eng. Sci.* **2010**, *50*, 191.
10. Wang, X. C.; Tzoganakis, S.; Rampel, G. L. *J. Appl. Polym. Sci.* **1996**, *61*, 1395.
11. Nofar, M.; Majithiya, K.; Kuboki, T.; Park, C. B. *J. Cell. Plast.* **2012**, *48*, 271.
12. Du, X. H.; Zhang, Z. J.; Yu, H. O.; Wan, D.; Xing, H. P.; Tang, T. *J. Appl. Polym. Sci.* **2010**, *115*, 1105.
13. Han, L.; Wang, Y.; Liu, L.; Xiang, F. M.; Huang, T.; Zhou, Z. W. *Chinese J. Polym. Sci.* **2010**, *28*, 457.
14. Li, S. Z.; Xiao, M. M.; Guan, Y.; Wei, D. F.; Xiao, H. N.; Zheng, A. N. *Eur. Polym. J.* **2012**, *48*, 362.
15. Zhang, Z. J.; Xing, H. P.; Qiu, J.; Jiang, Z. W.; Yu, H. O.; Du, X. H.; Wang, Y. H.; Ma, L.; Tang, T. *Polymer* **2010**, *51*, 1593.
16. Xing, H. P.; Jiang, Z. W.; Zhang, Z. J.; Qiu, J.; Wang, Y. H.; Ma, L.; Tang, T. *Polymer* **2012**, *53*, 947.
17. Zhang, Z. J.; Wan, D.; Xing, H. P.; Zhang, Z. J.; Tan, H. Y.; Wang, L.; Zheng, J.; An, Y. J.; Tang, T. *Polymer* **2012**, *53*, 121.
18. Wang, L.; Wan, D.; Zhang, Z. J.; Liu, F.; Xing, H. P.; Wang, Y. H.; Tang, T. *Macromolecules* **2011**, *44*, 4167.
19. Ma, G. Q.; Zhai, J. J.; Liu, B.; Huang, D. H.; Sheng, J. *Chinese J. Polym. Sci.* **2012**, *30*, 423.
20. Nojiri, A.; Sawasaki, T.; Koreeda T. U.S. Pat. 424, 293 (**1984**).
21. Pazzagli, F.; Pracella, M. *Macromol. Symp.* **2000**, *149*, 225.
22. Yi, X.; Xu, L.; Wang, Y. L.; Zhong, G. J.; Ji, X.; Li, Z. M. *Eur. Polym. J.* **2010**, *46*, 719.
23. Avilés, F.; Cauich-Rodríguez, J.V.; Moo-Tah, L.; May-Pat, A.; Vargas-Coronado, R. *Carbon* **2009**, *47*, 2970.
24. Pang, H.; Chen, C.; Bao, Y.; Chen, J.; Ji, X.; Lei, J.; Li, Z. M.; *Mater. Lett.* **2012**, *79*, 96.
25. Hwang, G. L.; Shieh, Y. T.; Hwang, K. C. *Adv. Funct. Mater.* **2004**, *14*, 487.

26. Ramanathan, T.; Fisher, F. T.; Ruoff, R. S.; Brinson, L. C. *Chem. Mater.* **2005**, *17*, 1290.

27. Li, W. H.; Chen, X. H.; Yang, Z.; Xu, L. S. *J. Appl. Polym. Sci.* **2009**, *113*, 3809.

28. Li, C. Q.; Deng, H.; Wang, K.; Zhang, Q.; Chen, F.; Fu, Q. *J. Appl. Polym. Sci.* **2011**, *121*, 2104.

29. Xu, J. Z.; Liang Y. Y.; Huang, H. D.; Zhong, G. J.; Lei, J.; Chen, C.; Li, Z. M. *J. Polym. Res.* **2012**, *19*, 9975.

30. Pang, H.; Zhong, G. J.; Xu, J. Z.; Yan, D. X.; Ji, X.; Li, Z. M.; Chen, C. *Chinese J. Polym. Sci.* **2012**, *30*, 879.

31. Menzer, K.; Krause, B.; Boldt, R.; Kretzschmar, B.; Weidisch, R.; Pötschke, P. *Compos. Sci. Technol.* **2011**, *71*, 1936.

32. Wang, L.; Wan, D.; Qiu, J.; Tang, T. *Polymer* **2012**, *53*, 4737.

33. Yan, D. X.; Xu, L.; Chen, C.; Tang, J. H.; Ji, Xu.; Li Z. M. *Polym. Int.* **2012**, *61*, 1107.